Rare-Earth Metal Cations Incorporated Silica Hybrid Nanoparticles Templated by Cylindrical Polymer Brushes

ARTICLE *in* CHEMISTRY OF MATERIALS · NOVEMBER 2013

Impact Factor: 8.35 · DOI: 10.1021/cm402776d

6 AUTHORS, INCLUDING:

Zhicheng Zheng
University of Bayreuth
8 PUBLICATIONS **28** CITATIONS
SEE PROFILE

Birgit Weber
University of Bayreuth
74 PUBLICATIONS **1,188** CITATIONS
SEE PROFILE

Axel H E Mueller
Johannes Gutenberg-Universität Mainz
590 PUBLICATIONS **17,825** CITATIONS
SEE PROFILE

CHEMISTRY OF MATERIALS

Article

pubs.acs.org/cm

Rare-Earth Metal Cations Incorporated Silica Hybrid Nanoparticles Templated by Cylindrical Polymer Brushes

Zhicheng Zheng,[‡] Alexander Daniel,[‡] Wei Yu,[†] Birgit Weber,[§] Jun Ling,*[,†,‡] and Axel H. E. Müller*[,‡,∥]

[†]MOE Key Laboratory of Macromolecular Synthesis and Functionalization, Department of Polymer Science and Engineering, Zhejiang University, Hangzhou 310027, China

[‡]Makromolekulare Chemie II, Universität Bayreuth, D-95440 Bayreuth, Germany

[§]Anorganische Chemie II, Universität Bayreuth, D-95440 Bayreuth, Germany

Supporting Information

ABSTRACT: A novel template-directed approach based on core−shell cylindrical polymer brushes (CPBs) has been developed to prepare rare-earth metal cations (Ln^{3+}) incorporated silica hybrid nanoparticles (NPs) with predictable dimensions. Tight chelation of Ln^{3+} ions in the core of the CPB template and a cross-linked silica layer deposited on the shell provide a very stable encapsulation of Ln^{3+} ions within the hybrid NPs and thus a high biocompatibility. As expected, the silica hybrid NPs obtain unique and diverse properties from the incorporated Ln^{3+} ions. That is, the hybrid NPs with Tb^{3+} or Eu^{3+} incorporation exhibit characteristic photoluminescence in visible light range, while the Gd^{3+}- and Tb^{3+}-containing hybrid NPs show paramagnetic behavior. Especially, the Gd^{3+}-containing silica hybrid NPs show a remarkable longitudinal relaxation time (T_1) shortening effect as well as minimal cytotoxicity, suggesting the application potential of these NPs as effective magnetic resonance imaging (MRI) contrast agents. This novel template-directed approach succeeds in combining different functional centers via loading in situ mixed Ln^{3+} ions (e.g. Tb^{3+} and Gd^{3+}) into individual CPBs resulting in multicomponent hybrid NPs, which possess both visible photoluminescence and T_1 contrast enhancement and can thus be applied as multimodal bioimaging probes.

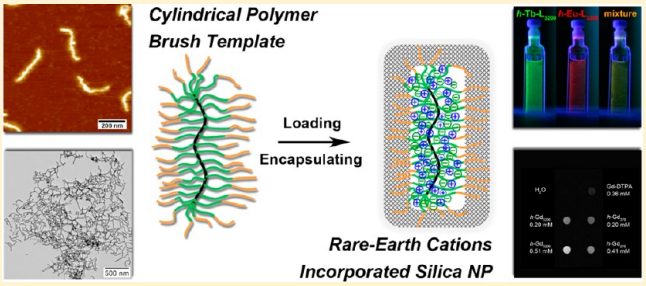

KEYWORDS: *rare-earth cations, cylindrical polymer brushes, template-directed, photoluminescence, paramagnetic, MRI contrast agent, cytotoxicity*

INTRODUCTION

Rare-earth metals, that is, the lanthanides from lanthanum (La) to lutetium (Lu), constitute a series of inner transition elements ("f-elements"). In the case of their trivalent cations (Ln^{3+}), the 4*f* orbital is filled in a completely regular manner from $4f^0$ for La^{3+} to $4f^{14}$ for Lu^{3+}. The shielding of the 4*f* electrons by the occupied $5s^2$ and $5p^6$ orbitals is responsible for the unique and diverse properties of the Ln^{3+} ions, which have encouraged scientists to use them as functional centers for constructing specific functional materials.[1,2] One important application is demonstrated in photonics, such as phosphors for displays and labels for bioimaging, since the luminescence of Ln^{3+} ions covers the spectral range from the ultraviolet to the near-infrared wavelength.[3−5] Lanthanide-doped luminescent nanomaterials possess high photostability,[6,7] no blinking,[8] sharp emission lines,[9] large Stokes shifts,[10] and long lifetimes of the emitting state.[10] Another well-known contribution of rare-earth ions is the application in developing magnetic materials, as several Ln^{3+} ions have a large number of unpaired electrons and thus provide high magnetic moments in a magnetic field.[11] Gd^{3+} ions with seven unpaired electrons can significantly decrease the relaxation time of water protons and are thus widely used as contrast agents for magnetic resonance imaging (MRI).[12] However, Gd^{3+} ions are highly toxic and must thus be chelated within ligands[13,14] or embedded in nanoparticles[15−20] to avoid the cytotoxicity for the MRI application.

In the past decade, core−shell(-corona) cylindrical polymer brushes (CPBs), providing a large number of chelating sites within their branched architectures, have been employed as templates for the preparation of various rod-like hybrid nanoparticles (NPs), such as magnetic hybrid NPs,[21,22] water-soluble organo-silica hybrid nanowires[23] and nanotubes,[24,25] cadmium sulfide hybrid NPs,[26] platinum-functionalized nanowires,[27] and titania hybrid NPs.[28,29] These template-directed prepared hybrid NPs obtain high dimensional stability from the core of the CPB, while the shell and/or corona protects them from agglomeration and precipitation in solution. In this work, we designed core−shell CPBs with poly(acrylic acid)-*block*-poly[2-(dimethylamino)ethyl methacrylate] (PAA-*b*-PDMAEMA) side chains, short as *b*-[AD], for the first time as templates

Received: August 18, 2013
Revised: October 17, 2013
Published: October 21, 2013

   dx.doi.org/10.1021/cm402776d | *Chem. Mater.* 2013, 25, 4585−4594

Scheme 1. Preparation of Well-Defined Rare-Earth Metal Cations (Ln^{3+}) Incorporated Silica Hybrid Nanoparticles via the Template-Directed Approach Based On Core-Shell Cylindrical Polymer Brushes

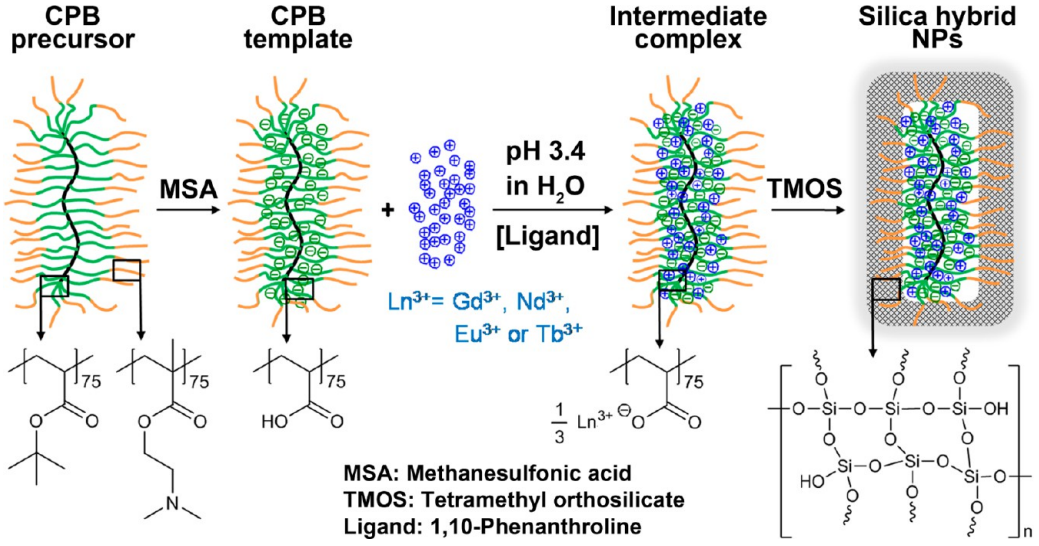

for the preparation of rare-earth metal cations (Ln^{3+}) incorporated hybrid NPs. As illustrated in Scheme 1, the CPB precursor with poly(*tert*-butyl acrylate)-*block*-PDMAEMA (P*t*BA-*b*-PDMAEMA) side chains, short as *b*-[TD], is converted into the CPB template *b*-[AD] *via* hydrolysis by methanesulfonic acid. Subsequently, various Ln^{3+} ions (i.e., gadolinium (Gd^{3+}), neodymium (Nd^{3+}), europium (Eu^{3+}), and terbium (Tb^{3+})) and their mixtures are incorporated into the PAA-core through an exchange between Ln^{3+} ions and hydrogen ions. A further localized deposition of tetramethyl orthosilicate (TMOS) molecules onto the PDMAEMA-shell and their subsequent condensation yield hybrid NPs with a cross-linked silica shell. The tight bonding of Ln^{3+} ions by the carboxylate ions in the PAA-core combined with the cross-linked silica shell ensures an isolating encapsulation of the toxic Ln^{3+} ions and thus a minimized cytotoxicity and a satisfying biocompatibility of the hybrid NPs.

EXPERIMENTAL SECTION

Materials. The synthesis of the macroinitiator poly[2-(2-bromoisobutyryloxy)ethyl methacrylate] (PBIEM, DP_n = 3200, PDI = 1.14) by anionic polymerization, acidic cleavage of the trimethylsilyl groups, and an esterification to attach the ATRP initiating sites was reported previously.[30] The monomer BIEM for synthesis of the other macroinitiator PBIEM with a DP_n of 270 was prepared according to literature method.[31] 2,2′-Azoisobutyronitrile (AIBN, 98%, Aldrich) was recrystallized from methanol. 2-Cyano-2-propyl benzodithioate (CPrB, RAFT agent, 97%, Aldrich), methanesulfonic acid (MSA, 99.5%, Aldrich) and tetramethyl orthosilicate (TMOS, 98%, Aldrich) were purchased and used without further treatment. CuBr (98%, Aldrich) was purified by stirring with acetic acid overnight. After filtration, it was washed with ethanol and diethyl ether and then dried in vacuum oven. *tert*-Butyl acrylate (*t*BA, 98%, Aldrich) and 2-(dimethylamino)ethyl methacrylate (DMAEMA, 98%, Aldrich) were purified by passing through basic alumina columns before polymerizations. Rare earth metal oxides (Nd_2O_3, Gd_2O_3, Eu_2O_3 and Tb_4O_7) were purchased from Beijing Founde Star Science and Technology Co. Ltd. and transformed to corresponding cations (Ln^{3+}) through reaction with acid at elevated temperature. All other solvents and chemicals were of analytical grade and used as received. Water was obtained from a Milli-Q PLUS (Millipore) apparatus.

Synthesis of Macroinitiator $PBIEM_{270}$. The macroinitiator $PBIEM_{270}$ was synthesized via RAFT polymerization of 2-(2-bromoisobutyryloxy)ethyl methacrylate (BIEM). RAFT agent 2-cyano-2-propyl benzodithioate (CPrB) (1.98 mg, 9.0×10^{-3} mmol), monomer BIEM (1.5 g, 5.4 mmol) and initiator AIBN (0.37 mg, 2.2×10^{-3} mmol) were dissolved in anisole. The reaction mixture was stirred and degassed with argon for 30 min and then heated to 70 °C. The polymerization was monitored by withdrawing samples for ^1H NMR measurements. When a desired conversion was achieved, the reaction was quenched by cooling the reaction mixture to room temperature and exposing it to air. The reaction mixture was purified by precipitating into cold *n*-hexane. DMAc-SEC (RI, PMMA calibration): M_n = 30.0 kDa, PDI = 1.21. ^1H NMR (300 MHz, $CDCl_3$, δ in ppm): 4.30 (s, 2H, $OCOCH_2C\underline{H}_2OCOC(CH_3)_2Br$), 4.14 (s, 2H, $OCOC\underline{H}_2CH_2OCOC(CH_3)_2Br$), 1.90 (s, 6H, $C(C\underline{H}_3)_2Br$), 1.25−0.70 (m, 3H, $CH_2CHC\underline{H}_3$).

Preparation of CPB Precursors *b*-[TD]. The homopolymer CPB *b*-$[T_{80}]_{270}$ was synthesized via ATRP from a $PBIEM_{270}$ backbone. A flask equipped with CuBr (15.4 mg, 1.07×10^{-1} mmol) and polyinitiator PBIEM (40 mg, 1.43×10^{-1} mmol initiating sites) was degassed with argon for 30 min. Then, degassed monomer *t*BA (7.35 g, 53.7 mmol) and solvent anisole were added by syringe. The mixture was stirred and heated to 60 °C. Finally, the degassed ligand, *N*,*N*,*N*′,*N*″,*N*″-pentamethyldiethylenetriamine (PMDETA, 18.6 mg, 1.07×10^{-1} mmol), was injected to start the polymerization, and an initial sample was taken for ^1H NMR measurement. The polymerization was monitored by withdrawing samples for ^1H NMR measurements. When a desired conversion was achieved, the reaction was quenched by cooling the reaction mixture to room temperature and exposing it to air. The reaction mixture was purified by passing through a silica gel column, followed by precipitating into cold methanol/water mixture (8:1) for twice. The initiating efficiency of the polyinitiator PBIEM toward *t*BA was determined as 65%. The procedure was detailed in our earlier work.[32] Based on the monomer conversion and the initiating efficiency, the DP_n of the P*t*BA block was calculated as 80. ^1H NMR (300 MHz, $CDCl_3$, δ in ppm): 1.38 (s, 9H, $OC(C\underline{H}_3)_3$).

The core−shell CPB *b*-$[T_{80}D_{77}]_{270}$ was obtained via ATRP of DMAEMA from the homopolymer CPB *b*-$[T_{80}]_{270}$. A round-bottom flask was charged with CuBr (3.32 mg, 2.32×10^{-2} mmol), *b*-$[T_{80}]_{270}$ (300 mg) and anisole. The mixture was degassed with argon for 30 min. After that, the degassed monomer DMAEMA (1.09 g, 6.95 mmol) was added by syringe into the flask, which was then heated to 90 °C. The degassed ligand PMDETA (4.01 mg, 2.32×10^{-2} mmol) was injected to start the polymerization. As described above, the polymerization was monitored by ^1H NMR measurements. After achieving a desired conversion, the reaction was quenched by cooling

dx.doi.org/10.1021/cm402776d | *Chem. Mater.* 2013, 25, 4585−4594

the reaction mixture to room temperature and exposing it to air. The reaction mixture was purified by passing through a silica gel column, followed by precipitating into cold *n*-hexane for twice. The DP_n of the PDMAEMA block was calculated as 77 from the ^1H NMR spectrum by comparing the *t*BA protons with the DMAEMA protons. ^1H NMR (300 MHz, $CDCl_3$, δ in ppm): 4.00 (s, 2H, $OC\underline{H}_2CH_2N(CH_3)_2$), 2.50 (s, 2H, $OCH_2C\underline{H}_2N(CH_3)_2$), 2.22 (s, 6H, $OCH_2CH_2N(C\underline{H}_3)_2$), 1.38 (s, 9H, $OC(C\underline{H}_3)_3$).

The core−shell CPB *b*-$[T_{75}D_{75}]_{3200}$ was prepared via the same approach as *b*-$[T_{80}D_{77}]_{270}$, with a $PBIEM_{3200}$ macroinitiator used as the backbone.

Preparation of CPB Templates *b*-[AD]. The core−shell CPB template *b*-$[A_{80}D_{77}]_{270}$ with a polyelectrolyte poly(acrylic acid) (PAA) core was synthesized via hydrolysis of the P*t*BA segments of the CPB precursor *b*-$[T_{80}D_{77}]_{270}$. Herein, *b*-$[A_{80}D_{77}]_{270}$ was dissolved in dichloromethane (about 15 mg/mL) and methanesulfonic acid (MSA)[33] was added at room temperature at a molar ratio of 20 compared to *t*BA units. After around 30 min, the solution became turbid. Stirring was continued for 24 h to ensure the full reaction. After evaporation of the organic solvent, the reaction product was dissolved in pure water.

The core−shell CPB template *b*-$[A_{75}D_{75}]_{3200}$ was prepared via the same approach as *b*-$[A_{80}D_{77}]_{270}$, with *b*-$[T_{75}D_{75}]_{3200}$ used as CPB precursor.

Preparation of Rare Earth Metal Cations Incorporated Silica Hybrid NPs. The Gd^{3+}-incorporated silica hybrid NP *h*-Gd_{270} was prepared via the template-directed approach. One milliliter aqueous solution of Gd^{3+} (0.22 mmol mL^{-1}) was added into 3.4 mL aqueous solution of CPB template *b*-$[A_{80}D_{77}]_{270}$ (1.0 mg mL^{-1}) under stirring. The pH-value and the temperature of the solution were kept at 3.4−3.6 and 15 °C, respectively. 0.2 mL of tetramethyl orthosilicate (TMOS) was added into the solution under stirring.[34,35] The deposition and cross-linking procedure of TMOS on the PDMAEMA segments was running for 20 min. The achieved silica hybrid NP *h*-Gd_{270} was purified by ultracentrifugation. The precipitates were washed with ethanol, redissolved in ethanol using ultrasonic bath and ultracentrifuged for three times.

The silica hybrid NPs *h*-Gd_{3200}, *h*-Nd_{3200}, *h*-Nd_{270}, *h*-Tb_{3200} and *h*-Tb_{270} were prepared via the same template-directed approach as *h*-Gd_{270}, with corresponding CPB template and Ln^{3+} aqueous solution being applied. In the preparation of the ligand-coordinating hybrid NPs *h*-Tb-L_{3200} and *h*-Eu-L_{3200}, 1,10-phenanthroline (50 mg, 0.28 mmol) as ligand was added into the reaction solution before the adding of TMOS. In the case of multicomponent hybrid NPs *h*-Tb/Gd_{3200} and *h*-Tb/Nd_{3200}, corresponding Ln^{3+} mixture was used for the template-directed synthesis.

Characterization Methods. *Size Exclusion Chromatography (SEC).* SEC was conducted by using dimethyl acetamide (DMAc) with 0.05% lithium bromide as eluent at an elution rate of 0.8 mL min^{-1}. The equipment consists of one precolumn and two analytical columns (PSS GRAM, 10^2 and 10^3 Å pore size, 7 mm particle size) and an Agilent 1200 RI detector. The measurements were performed at 60 °C. PMMA calibration curve was used to calibrate the columns.

^1H Nuclear Magnetic Resonance Spectroscopy (^1H NMR). ^1H NMR measurements were carried out on a Bruker AC-300 instrument at room temperature in $CDCl_3$.

Tapping-mode Atomic Force Microscopy (AFM). AFM images were recorded on a Digital Instruments Dimension 3100 microscope operated in tapping mode. The samples were prepared by spin-coating (3000 rpm, 1 min) diluted aqueous solutions onto freshly cleaved mica surface.

Transmission Electron Microscopy (TEM). TEM images of silica hybrid NPs were recorded on Zeiss CEM 902 and LEO 922 OMEGA electron microscopes operated at 80 kV and 200 kV, respectively. Data evaluation and processing was carried out with Soft Imaging Viewer and Image Tool. A 2 μL droplet of the ethanol solution of silica hybrid NPs was dropped onto a copper grid coated with carbon film, followed by a removal of the redundant solution using a filter paper.

Scanning Electron Microscopy (SEM) and Energy Dispersive X-ray (EDX) Analysis. SEM was performed by using a Zeiss Leo 1530 instrument equipped with a field emission cathode with a lateral resolution of approximately 2 nm. The sample was measured after sputtering a thin layer (1−2 nm) of platinum. EDX analysis was performed by using an Oxford EDX INCA 400 detector and a Thermo Fischer Scientific Noran System 7 with corresponding NSS 3 X-ray MicroAnalysis software.

Thermogravimetric Analysis (TGA). TGA was conducted on a Mettler Toledo TGA/SDTA 85 instrument under a constant air flow of 60 mL min^{-1}. The measurements were scanned in the temperature range 30−700 °C at a heating rate of 10 K min^{-1}.

Inductively Coupled Plasma Optical Emission Spectrometry (ICP-OES). ICP-OES was applied to determine the rare earth metal cation (Ln^{3+}) contents of the silica hybrid NPs. The measurements were conducted on a Varian Vista-Pro Radial instrument. Standard solutions of free rare earth metal cations (1 g L^{-1}) were prepared as the references for the measurements.

Leaching Study of Ln^{3+} from Silica Hybrid NPs. The stability of the encapsulation of Ln^{3+} within the silica hybrid NPs *h*-Gd_{3200} and *h*-Tb_{3200} was determined by performing a complexometric titration of free Ln^{3+} leaching from the hybrid NPs, using xylenol orange as indicator. Xylenol orange gives a yellow color in a noncomplex form (λ_{max} = 432 nm in UV−vis absorption spectrum), while a red color is observed from the complex of xylenol orange with Ln^{3+}. By measuring the absorption at the wavelength of 432 nm, a quantitative analysis of free Ln^{3+} is feasible. Xylenol orange solution was prepared by dissolving 36 mg of xylenol orange tetrasodium salt (3,3′-bis[*N*,*N*-bis(carboxymethyl)aminomethyl]-*o*- cresolsulfonephthalein tetrasodium salt) in 100 mL acetate puffer (sodium acetate/acetic acid, pH 5.8). The obtained xylenol orange solution was kept in 1 mL portion in 1.5 mL Eppendorf PCR centrifuge vials at −30 °C. The procedure of the complexometric titration: 1.5 mL of *h*-Gd_{3200} solution (output $[Gd^{3+}]$ = 0.7 mM) was centrifuged for 10 min. The precipitates were isolated and redissolved in 1.5 mL water. The start of the redissolving is defined as the zero point of the kinetic measurement of the leaching study of Ln^{3+}. After a time period *t* (1 h, 1 d, 3 d, 7 d, or 14 d), an 250 μL aliquot solution was taken, diluted in 1 mL water and centrifuged for 10 min. Now, 250 μL of the supernatant solution was taken and diluted in 5 mL water. The obtained solution was filtered through a 0.2 μm nylon filter. Then, 100 μL of the filtrate was added into a mixture of 2.8 mL acetate puffer and 100 μL xylenol orange indicator solution. The obtained solution was transferred completely into a quartz cuvette and measured for its adsorption in the range 200−800 nm by using a Hitachi U-3000 UV−vis spectrometer. A control sample containing acetate puffer and xylenol orange indicator but without hybrid NP was also measured. A working curve of the adsorption depending on the Tb^{3+}-concentration was measured previously from a concentration series of free Tb^{3+} in water (0.3−9 μM). The complexometric titration *h*-Tb_{3200} solution (output $[Tb^{3+}]$ = 0.5 mM) was performed in the same way.

Photoluminescence (PL) Spectroscopy. PL excitation and emission spectra of the ethanol solutions of the Tb^{3+}- and Eu^{3+}-containing silica hybrid NPs were recorded by using a Shimadzu RF-5301 PC fluorescence spectrometer. The Ln^{3+}-concentration of each sample was previously determined by ICP-OES, as described above. A UV lamp operating at 266 nm was applied to record the luminescence images of the ethanol solutions of hybrid NPs.

Superconducting Quantum Interference Device (SQUID) Magnetometer. SQUID measurements of the Gd^{3+}- and Tb^{3+}-containing silica hybrid NPs were performed on a Quantum Design MPMS-XL-5 SQUID magnetometer. About 10 mg of hybrid NPs was dried in a gelatin capsule for the measurement. The magnetizations of the hybrid NPs were measured as function of the applied magnetic field with a maximal strength of 5 T at 5 K in the hysteresis mode. Temperature-dependent magnetizations of the hybrid NPs were scanned in the temperature range of 2 − 300 K with an applied magnetic field strength of 1 T.

Relaxivity Measurements of Gd^{3+}-Containing Silica Hybrid NPs. The longitudinal T_1 and transverse relaxation time T_2 of Gd^{3+}-containing silica hybrid NPs were measured on a Bruker Ultrashield 300 MHz instrument at 37 °C and 7.0 T. For each type of hybrid NPs,

dx.doi.org/10.1021/cm402776d | *Chem. Mater.* 2013, 25, 4585−4594

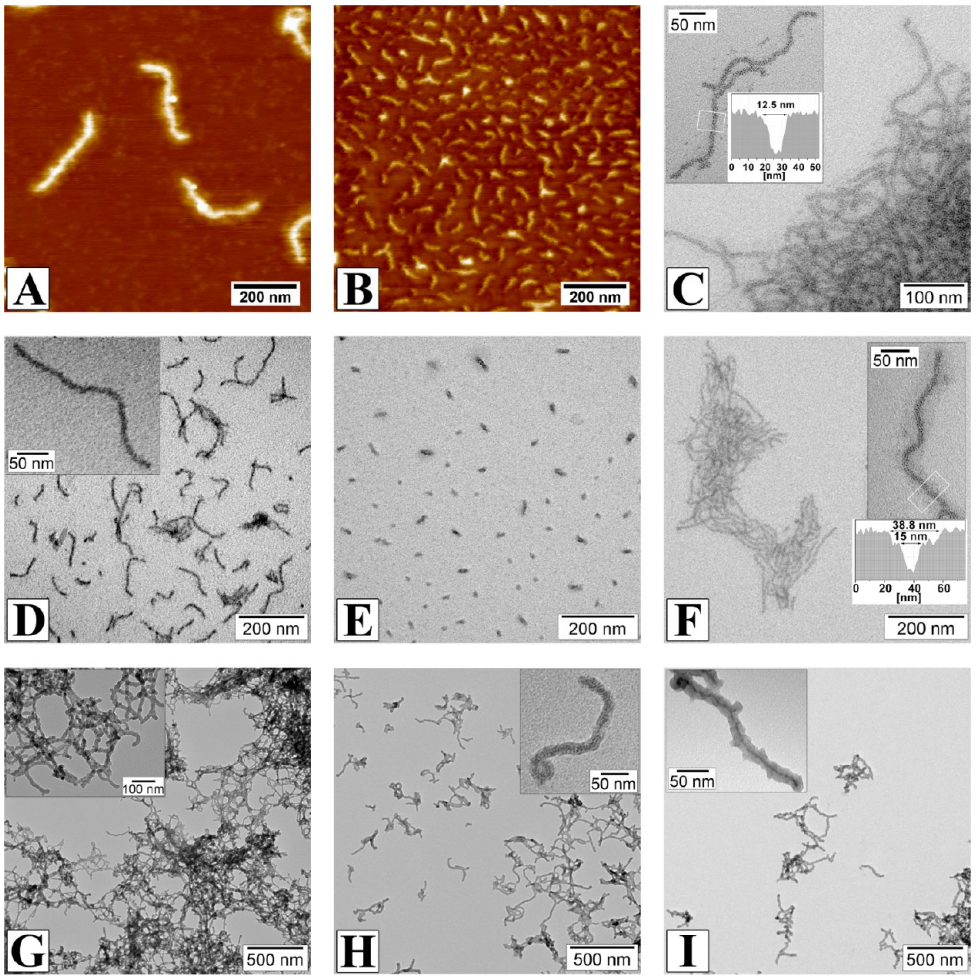

Figure 1. Tapping-mode AFM height image of the longer CPB precursor *b*-$[T_{75}D_{75}]_{3200}$ (A) and the shorter CPB precursor *b*-$[T_{80}D_{77}]_{270}$ (B). TEM image of the Gd^{3+}-loaded template intermediate without silicate deposition (C), the Ln^{3+}-incorporated silica hybrid NPs *h*-Gd_{3200} (D), *h*-Gd_{270} (E), *h*-Tb_{3200} (F), the ligand-coordinating silica hybrid NPs *h*-Tb-L_{3200} (G), and *h*-Eu-L_{3200} (H), and the multicomponent silica hybrid NP *h*-Tb/Gd_{3200} (I). The insets in C and F show the grayscale analysis of the marked areas.

a concentration series (0.01−0.8 mM of Gd^{3+} in D_2O) was prepared and previously determined by ICP-OES, as described above. T_1 and T_2 were determined for three times by applying Inversion−Recovery pulse sequence and Car-Purcell-Meilboom-Gill pulse sequence, respectively. The inverses of the mean of T_1 and that of T_2, namely the relaxation rates $1/T_1$ and $1/T_2$, were plotted versus the Gd^{3+}-concentration of the hybrid NPs to calculate their relaxivities r_1 and r_2, that is, the slopes of the plots.

MRI Phantom Study of Gd^{3+}-Containing Silica Hybrid NPs. The T_1-weighted MRI images of Gd^{3+}-containing silica hybrid NPs were acquired on a GE Signa MRI 3.0 T Scanner at room temperature. Samples of *h*-Gd_{270} and *h*-Gd_{3200} were prepared in deionized water with concentrations of 0.20, 0.41 mM and 0.20, 0.51 mM of total Gd^{3+}, respectively. A sample of pure deionized water and another sample of commercial contrast agent gadopentetate dimeglumine (Gd-DTPA) with a Gd^{3+}-concentration of 0.36 mM in deionized water were measured as references. The parameters of the measurements are given as follows: a repetition time (TR) of 60 ms, an echo time (TE) of 11 ms, a slice thickness of 1.0 mm, a spacing of 0.5 mm, a FOV read of 70 mm, and an 8 h brain small coil with an inner diameter of 50 mm.

Cell Culture. The human bronchoalveolar carcinoma derived cell line A549 cells were obtained from Cell Bank of Typical Culture Collection of Chinese Academy of Sciences (Shanghai, China) and maintained in regular growth medium consisting of high glucose DMEM supplemented with 10% fetal bovine serum (FBS), 100 μL penicillin, and 100 μg mL^{-1} streptomycin at 37 °C, in a 5% CO_2 humidified incubator. The human endothelial cells (CRL-1730) were obtained from American Type Culture Collection (ATCC, USA) and maintained with regular growth medium consisting of high-glucose RPMI 1640 supplemented with 10% FBS, 100 μL penicillin, and 100 μg mL^{-1} streptomycin, and cultured at 37 °C in a 5% CO_2 humidified environment. The cells were routinely passaged until 80−90% confluence. Briefly, the culture medium was removed and the cells were carefully washed three times with phosphate buffered saline (PBS) to remove all traces of serum which contains trypsin inhibitor. The cells were then incubated with 1 mL trypsin/ethylenediaminetetraacetic acid disodium salt (EDTA, 0.25%) in PBS until the cell layer was dispersed (usually within 5 min). The trypsin was blocked by adding 6.0−8.0 mL complete growth medium and the cells were aspirated by gentle pipetting. The cells were isolated by centrifugation at 1000 rpm for 5 min and then dispersed in fresh culture medium and incubated at 37 °C.

Cytotoxicity Study of Gd^{3+}-Containing Silica Hybrid NPs. The A549 cells were plated at a density of 1×10^4 cells per well on a 96-well plate and cultured for 16 h for the cell viability assay. The medium was replaced with fresh one containing the hybrid NPs of variable concentrations. To determine the cell viability, after coincubation with the hybrid NPs for determined time intervals (24 or 72 h), 20 μL 3-[4,5-dimethylthiazol-2-yl]-2,5-diphenyltetrazolium bromide (MTT, 5 mg mL^{-1}) was added to each well and the cells were continuously cultured at 37 °C for 4 h. The dark blue formazan crystals generated by the mitochondria dehydrogenase in viable cells were dissolved in dimethyl sulphoxide (DMSO), whose absorbance was measured at 570 nm by a microplate reader (Biorad Model 680). Three parallel

dx.doi.org/10.1021/cm402776d | *Chem. Mater.* 2013, 25, 4585−4594

experiments were conducted, and the data were normalized to that of the hybrid NP-free control. The endothelial cells were cultured in a 96-well plate until 80−90% confluence for cell viability study. The medium was replaced with fresh one containing the hybrid NPs of variable concentrations. To determine the cell viability, after the cells were coincubated with the hybrid NPs for 24 or 72 h, 20 μL MTT (5 mg mL^{-1}) was added to each well and the cells were further cultured at 37 °C for 4 h. The cell viability was determined with the same method as that for A549 cells.

RESULTS AND DISCUSSION

Synthesis of Ln^{3+} Incorporated Hybrid NPs. Two core−shell CPB precursors *b*-[TD] with different lengths were synthesized via sequential grafting of P*t*BA and PDMAEMA blocks using ATRP from well-defined polyinitiators poly[2-(2-bromoisobutyryloxy)ethyl methacrylate] (PBIEM) with degrees of polymerization, DP, of 3200 (polydispersity index, PDI = 1.14) and 270 (PDI = 1.21), respectively. The synthetic route is illustrated in Scheme S1 (Supporting Information (SI)). The longer CPB precursor was determined to have 75 P*t*BA and 75 PDMAEMA units in its block copolymer side chains (short as *b*-$[T_{75}D_{75}]_{3200}$), whereas the shorter CPB precursor was defined as *b*-$[T_{80}D_{77}]_{270}$ according to ^{1}H NMR analyses shown in Figure S1 (SI). Tapping-mode atomic force microscopy (AFM) shows that the CPB precursors *b*-$[T_{75}D_{75}]_{3200}$ and *b*-$[T_{80}D_{77}]_{270}$ have worm-like conformations with the number-average length, L_n, of 313 ± 62 nm (Figure 1A and Figure S2B (SI)) and 52 ± 9 nm (Figure 1B and Figure S2E (SI)), respectively. Acidic hydrolysis of the CPB precursors *b*-[TD] formed CPB templates with PAA-*b*-PDMAEMA side chains, *b*-$[A_{75}D_{75}]_{3200}$ and *b*-$[A_{80}D_{77}]_{270}$, whose AFM images are shown in Figures S2C and S2F (SI).

By employing the CPB templates, various Ln^{3+}-incorporated hybrid NPs were successfully prepared via a loading and encapsulation process, as given in Table 1. They are single-component silica hybrid NPs *h*-Gd_{3200}, *h*-Gd_{270}, *h*-Nd_{3200}, *h*-Nd_{270}, *h*-Tb_{3200}, and *h*-Tb_{270}, ligand-coordinating ones *h*-Tb-L_{3200} and *h*-Eu-L_{3200} (1,10-phenanthroline as ligand), as well as multicomponent ones *h*-Tb/Gd_{3200} and *h*-Tb/Nd_{3200} (loaded with Ln^{3+} mixtures). In the loading process, the pH was kept at 3.4, where the PDMAEMA segments are almost completely protonated and strongly positively charged. Therefore, their ability to form complex with metal cations (also positively charged) is strongly reduced. In contrast, the PAA units are still capable to chelate the metal cations at this pH. In the silica encapsulation, the partially negatively charged silicate precursor TMOS is first adsorbed on the positively charged PDMAEMA segments, which catalyze the hydrolysis of TMOS to orthosilicic acid ($Si(OH)_4$). A following condensation into silica finishes the encapsulation. Since we conducted this loading and encapsulation process in excess of Ln^{3+} ions and TMOS, every template brush adsorbed sufficient silicate precursor on its shell and underwent a complete encapsulation. Both the silica hybrid NPs derived from *b*-$[A_{75}D_{75}]_{3200}$ and that from *b*-$[A_{80}D_{77}]_{270}$ maintain the cylindrical worm-like conformations from the templates as demonstrated in the transmission electron microscopy (TEM) images (Figure 1D−I), with the former and the latter NPs having $L_n \approx 200$ and 50 nm, respectively (Table 1). The silica hybrid NPs have a core−shell nanostructure with a dark Ln^{3+}-containing core (more electron-dense) and a gray silica shell (Figures 1F and 1I for *h*-Tb_{3200} and *h*-Tb/Gd_{3200}), while the intermediate of Gd^{3+}-loaded *b*-$[A_{75}D_{75}]_{3200}$ without deposition of TMOS shows only a homogeneous dark nanostructure (Figure 1C).

Table 1. Silica Hybrid Nanoparticles with Different Rare-Earth Metal Cations (Ln^{3+}) Incorporations and Dimensions

hybrid	brush template	length[b] [nm]	Ln^{3+} content[c] [wt %]
h-Gd_{3200}	*b*-$[A_{75}D_{75}]_{3200}$	194 ± 24	12.0
h-Gd_{270}	*b*-$[A_{80}D_{77}]_{270}$	51 ± 5	6.5
h-Nd_{3200}	*b*-$[A_{75}D_{75}]_{3200}$	191 ± 30	10.0
h-Nd_{270}	*b*-$[A_{80}D_{77}]_{270}$	46 ± 5	6.8
h-Tb_{3200}	*b*-$[A_{75}D_{75}]_{3200}$	196 ± 57	12.0
h-Tb_{270}	*b*-$[A_{80}D_{77}]_{270}$	48 ± 5	6.9
h-Tb-L_{3200}[a]	*b*-$[A_{75}D_{75}]_{3200}$	221 ± 51	8.1
h-Eu-L_{3200}[a]	*b*-$[A_{75}D_{75}]_{3200}$	212 ± 37	8.4
h-Tb/Gd_{3200}	*b*-$[A_{75}D_{75}]_{3200}$	238 ± 38	5.2/4.3
h-Tb/Nd_{3200}	*b*-$[A_{75}D_{75}]_{3200}$	194 ± 31	4.6/4.2

[a]L stands for 1,10-phenanthroline as ligand. [b]Measured from TEM images. [c]Determined by ICP-OES.

The Ln^{3+}-contents of the silica hybrid NPs were determined by inductively coupled plasma optical emission spectrometry (ICP-OES) as 9−12% for the NPs derived from the CPB template *b*-$[A_{75}D_{75}]_{3200}$ and 6−7% for the ones from *b*-$[A_{80}D_{77}]_{270}$ (Table 1). This lower Ln^{3+} content of the shorter NPs is attributed to the increased surface-to-volume ratio, which shifts the silica-to-Ln^{3+} ratio in favor of silica, as more silicate precursors deposited and condensed on the shell. It is to note that in the multicomponent hybrid NPs *h*-Tb/Gd_{3200} and *h*-Tb/Nd_{3200}, each component has almost the same content. By combining the ICP-OES results with the TGA measurements (Figure S3, SI), the weight fraction of the silica shell in the silica hybrid NPs was determined as ca. 11%. Furthermore, scanning electron microscopy (SEM) images with combined energy-dispersive X-ray (EDX) analysis of the silica hybrid NPs also qualitatively confirms the Ln^{3+}-loading and the silica encapsulation of the hybrid NPs, as shown in Figure S4 (SI). The stability of the encapsulation of Ln^{3+} ions within the silica hybrid NPs was confirmed by measuring the leaching kinetic of Ln^{3+} ions from the NPs via a complexometric titration using xylenol orange as indicator. After dissolving in water for 14 d, the concentration of free Ln^{3+} ions in the solutions of hybrid NPs *h*-Gd_{3200} (output $[Gd^{3+}]$ = 0.7 mmol L^{-1}) and *h*-Tb_{3200} (output $[Tb^{3+}]$ = 0.5 mmol L^{-1}) maintained below the detection limit of 0.01 mmol L^{-1} (Figure S5, SI). Compared with other reported Ln^{3+}-nanosystems,[16,36] our silica hybrid NPs provide a very stable encapsulation of the toxic Ln^{3+} ions, indicating application potential as stable and safe nanomaterials. In addition, the silica shell ensures excellent solubility of the silica hybrid NPs in water and alcohols. This is confirmed by the dynamic light scattering (DLS) measurement of the hybrid NP *h*-Tb_{3200} in aqueous solution, which demonstrates a monomodal and narrow particle size distribution with average apparent hydrodynamic radius, $R_{h,app}$, of 247 nm and a dispersity index, DI, of 0.18, as shown in Figure S6 (SI).

Visible Photoluminescence of the Hybrid NPs with Tb^{3+} or Eu^{3+} Incorporation. Nanoparticles with visible luminescence (wavelength from 390 to 700 nm) are of great interest in the research and development of display screens, sensors, and light-emitting diodes. The prepared silica hybrid NPs with Tb^{3+} or Eu^{3+} incorporation are expected to be photoluminescent in the visible range. Upon excitation at 292 nm, *h*-Tb_{3200} emits much stronger luminescence in ethanol solution (c_{Tb} = 80 mg L^{-1}) at the Tb^{3+} characteristic wavelengths of 488 nm (energy level transition: $^5D_4 \rightarrow {}^7F_6$)

dx.doi.org/10.1021/cm402776d | Chem. Mater. 2013, 25, 4585−4594

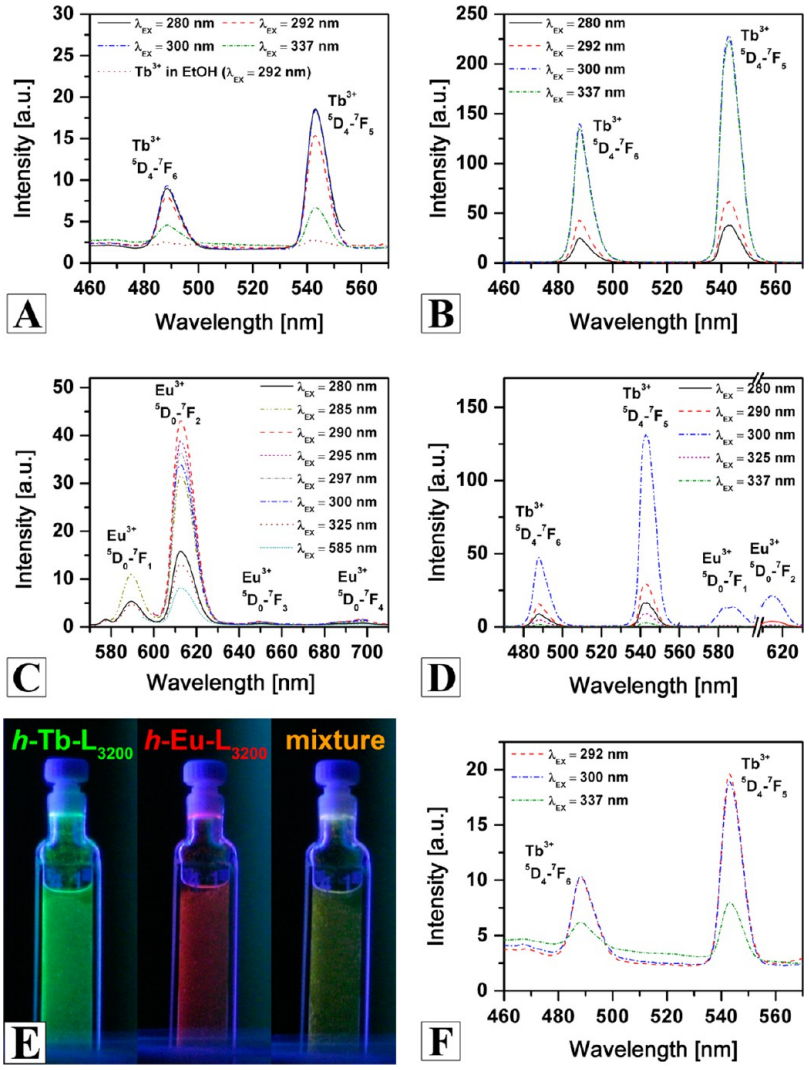

Figure 2. Photoluminescence emission spectra of the silica hybrid NPs in ethanol solution upon exciting at different wavelengths: *h*-Tb_{3200} with c_{Tb} = 80 mg L^{-1} (A), *h*-Tb-L_{3200} with 1,10-phenanthroline as ligand, c_{Tb} = 160 mg L^{-1} (B), *h*-Eu-L_{3200} with c_{Eu} = 82 mg L^{-1} (C), a mixed solution of *h*-Tb-L_{3200} and *h*-Eu-L_{3200} with c_{Tb} = 32 mg L^{-1}, c_{Eu} = 65 mg L^{-1} (D) and the multicomponent hybrid NPs *h*-Tb/Gd_{3200} with c_{Tb} = 47 mg L^{-1}, c_{Gd} = 45 mg L^{-1} (F). The brown dash line in A corresponds to the emission spectrum of an ethanol solution of free Tb^{3+} cations with c_{Tb} = 3600 mg L^{-1}. Luminescence image of the ethanol solutions of *h*-Tb-L_{3200}, *h*-Eu-L_{3200} and their mixture under excitation at 266 nm (E).

and 543 nm ($^5D_4 \rightarrow {}^7F_5$) than free Tb^{3+} ions (c_{Tb}= 3600 mg L^{-1}), as shown in Figure 2A. This means the bonding of Tb^{3+} in the PAA-core and the isolation by the silica shell in the hybrid NP are able to avoid solvent-induced quenching. Several wavelengths chosen from the excitation spectrum (Figure S7A, SI) were applied to excite *h*-Tb_{3200}, and we found that the excitation wavelengths of 280 and 300 nm induce the highest luminescence. The emission spectrum of *h*-Tb-L_{3200} in ethanol solution (c_{Tb} = 160 mg L^{-1}) indicates that the introduction of a ligand, 1,10-phenanthroline, enhances the luminescence of Tb^{3+} ions (Figure 2B), especially for the excitation at 300 and 337 nm, as the luminescence is 10 times higher than that of the *h*-Tb_{3200} solution. This sensitization effect is attributed to a more efficient light absorption of the Tb^{3+} ions coordinated by the ligand.[37,38] Furthermore, since 1,10-phenanthroline is a neutral ligand, there is no interaction between the ligand and the brushes so that it does not influence the Coulombic interaction between the Ln^{3+} ions and the PAA core. Another silica hybrid NP, *h*-Eu-L_{3200}, succeeds in emitting luminescence of Eu^{3+} ions in ethanol solution (c_{Eu}= 82 mg L^{-1}) at the characteristic wavelengths of 590 nm ($^5D_0 \rightarrow {}^7F_1$), 615 nm ($^5D_0 \rightarrow {}^7F_2$), 650 nm ($^5D_0 \rightarrow {}^7F_3$), and 702 nm ($^5D_0 \rightarrow {}^7F_4$), with 290 and 295 nm being the most effective excitation wavelengths (Figure 2C).

Mixing the hybrid NPs *h*-Tb-L_{3200} and *h*-Eu-L_{3200} in ethanol solution (c_{Tb}:c_{Eu} = 1:2) demonstrates a straightforward way to combine different functional centers. In the emission spectrum of this mixed solution, both the luminescence of Tb^{3+} ions (488 nm, 543 nm) and that of Eu^{3+} ions (590 nm, 615 nm) are observed (Figure 2D), indicating that the separated encapsulation of Tb^{3+} and Eu^{3+} ions avoids interference between their photoluminescent behavior. The luminescence image confirms the functionality combination, as *h*-Tb-L_{3200} and *h*-Eu-L_{3200} in ethanol solution shows a green and a red color, respectively, while a further yellow color was observed in the mixed solution (Figure 2E). Another way to combine different functional centers is demonstrated by the multicomponent hybrid NP *h*-Tb/Gd_{3200} with incorporation of a mixture of Tb^{3+} and Eu^{3+} ions. This multicomponent hybrid NP with a lower Tb^{3+} concentration (c_{Tb}= 47 mg L^{-1} and c_{Gd}= 45 mg L^{-1}) in

dx.doi.org/10.1021/cm402776d | *Chem. Mater.* 2013, 25, 4585−4594

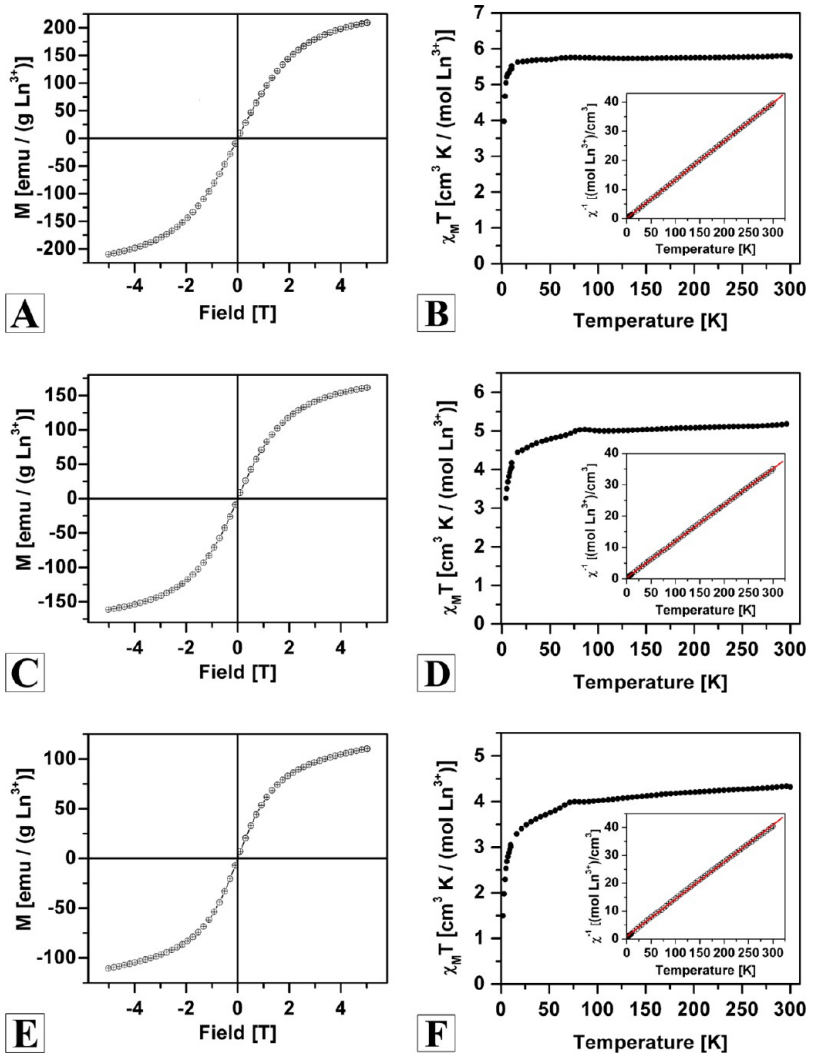

Figure 3. Magnetization curves at 5 K for the silica hybrid NPs h-Gd_{3200} (A), the multicomponent hybrid NPs h-Tb/Gd_{3200} (C), and h-Tb/Nd_{3200} (E). Temperature dependence of the product of molar susceptibility and temperature ($\chi_M T$) at 1 T for h-Gd_{3200} (B), h-Tb/Gd_{3200} (D), and h-Tb/Nd_{3200} (F). The inset shows the temperature dependence of the inverse susceptibility (χ_M^{-1}). Black cycles, experimental results; red line, Curie fitting result.

ethanol solution exhibits the same high luminescence as the h-Tb_{3200} solution (Figure 2F vs A). This luminescence sensitization effect induced by an effective metal-to-metal energy transfer (Gd^{3+}:$^6P_J \rightarrow Tb^{3+}$:$^5H_J$)[39] indicates that the in situ mixed loading of various Ln^{3+} ions into individual NP provides possibilities for interactions among different functional centers.

By comparing the excitation and the emission spectra of the longer NP h-Tb_{3200} (Figures S7A (SI) and 2A) with that of the shorter NP h-Tb_{270} (Figures S7E and F, SI), the influence of the NP size on the photoluminescence behavior was investigated. Both NPs possess excitation and luminescence at the same wavelengths, suggesting no effect of the NP size on the energy band gap and thus the luminescence behavior. That is due to the same chemical environment of Ln^{3+} ions within various NPs, which is independent of the NP size.

Magnetic Behavior of the Gd^{3+}- and Tb^{3+}-Containing Hybrid NPs. The Gd^{3+}- and Tb^{3+}-containing silica hybrid NPs were investigated for their potential magnetic properties by superconducting quantum interference device (SQUID) measurements. The magnetization curves at a temperature of 5 K and the temperature dependence of the molar magnetic susceptibility (χ_M) at an external field of 1 T for h-Gd_{3200}, h-Tb/Gd_{3200}, and h-Tb/Nd_{3200} are shown in Figure 3, with the main results given in Table 2. The magnetization of h-Gd_{3200} rises with increasing applied field strength without any hysteresis indicating a paramagnetic behavior at 5 K (Figure 3A). Fitting with the Langevin function (Figure S8A, SI) leads to a saturation magnetization, M_s = 266.1 emu/(g Ln^{3+}), which coincides with the theoretical value for free Gd^{3+} ions (249

Table 2. Magnetic Properties of the Gd^{3+}- and Nd^{3+}-Containing Silica Hybrid NPs

hybrid	M_s[a] [emu/(g Ln^{3+})]	C[b] [cm^3 K/(mol Ln^{3+})]	θ[b] [K]	μ_{eff}[c] [μ_B]
h-Gd_{3200}	266.1	7.58	−0.8	6.80
h-Tb/Gd_{3200}	210.2	8.65	−3.5	6.44
h-Tb/Nd_{3200}	145.2	7.50	−6.9	5.88

[a]Saturation magnetization at 5 K obtained by fitting the magnetization curve with the Langevin function. [b]Curie constant (C) and Weiss constant (θ) determined by fitting the inverse susceptibility (χ_M^{-1}) vs temperature curve at 1 T. [c]Effective magnetic moment calculated from the product of molar susceptibility and temperature ($\chi_M T$) at 300 K.

dx.doi.org/10.1021/cm402776d | Chem. Mater. 2013, 25, 4585−4594

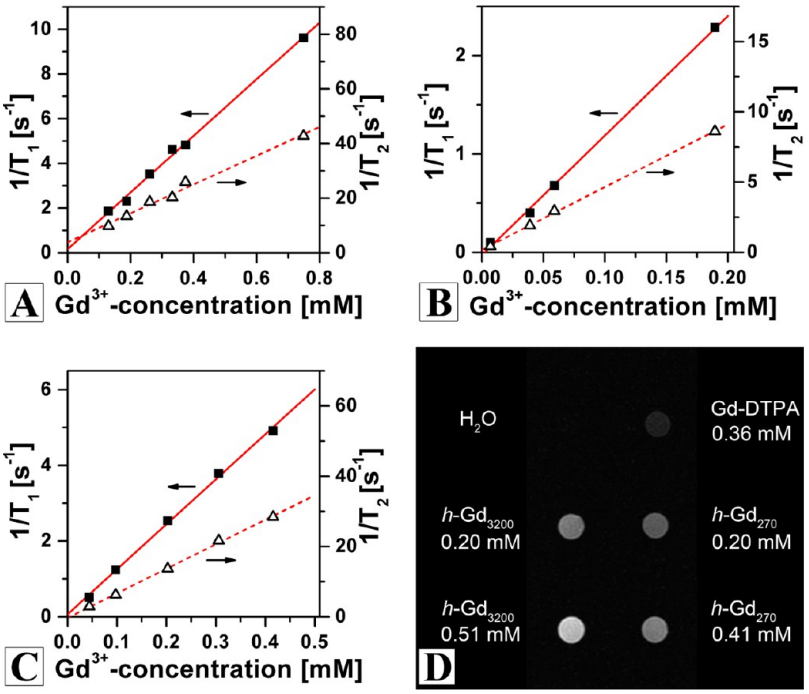

Figure 4. Plots of longitudinal ($1/T_1$) and transverse relaxation rate ($1/T_2$) versus Gd^{3+}-concentration of the silica hybrid NPs h-Gd_{3200} (A), h-Gd_{270} (B) and the multicomponent hybrid NPs h-Tb/Gd_{3200} (C) in D_2O at 37 °C and 7 T. T_1-weighted MRI images of h-Gd_{3200} and h-Gd_{270} with different Gd^{3+}-concentrations (D). Deionized water and commercial contrast agent Gd-DTPA were measured as references.

emu/(g Ln^{3+})). The plot of the $\chi_M T$ product as a function of temperature in the range of 2 to 300 K (Figure 3B) suggests a classic paramagnetic behavior of h-Gd_{3200}. The effective magnetic moment, μ_{eff}, at 300 K was determined as 6.80 μ_B, which is slightly lower than the theoretical value for free Gd^{3+} ions (7.94 μ_B). The inverse susceptibility, χ_M^{-1}, of h-Gd_{3200} shows a perfect linear dependence on the temperature over the full range (Figure 3B, inset). A Curie fitting of this plot suggests a Curie constant C = 7.58 cm^3 K/(mol Ln^{3+}) and a Weiss constant θ = −0.8 K (Table 2). This almost negligible Weiss constant also indicates an ideal paramagnetic Curie behavior of h-Gd_{3200}. All the magnetic properties of h-Gd_{3200} discussed above imply that the individual Gd^{3+} ions in the NP are isolated from each other possessing independent atomic moments. In the case of multicomponent hybrid NPs h-Tb/Gd_{3200} and h-Tb/Nd_{3200}, the magnetization curves at 5 K also follow a paramagnetic manner (Figures 3C and E). Compared with h-Gd_{3200}, the incorporation of Tb^{3+} in h-Tb/Gd_{3200} slows down the increase of magnetization with increasing field strength (Figure 3C). An M_s of 210.2 emu/(g Ln^{3+}) is extrapolated using the Langevin function (Figure S8B, SI), which is lower than the theoretical value for independently acting Tb^{3+} and Gd^{3+} ions (285 emu/(g Ln^{3+})). This could be an indication for some cooperative interactions between the ions in the NP at 5 K, which could be communicated through the carboxylate groups. This phenomenon is also observed in other multicomponent hybrid NP h-Tb/Nd_{3200}, as an M_s of 145.2 emu/(g Ln^{3+}) is expected (Figure 3E and Figure S8C (SI)), which is lower than the theoretical value (225 emu/(g Ln^{3+})). However, the effect is very small as the characteristics, μ_{eff} at 300 K, C and θ, determined from the temperature dependence of $\chi_M T$ and χ_M^{-1} (Figures 3D and F, Table 2) confirm an almost ideal Curie paramagnetic behavior of h-Tb/Gd_{3200} and h-Tb/Nd_{3200}.

Relaxation Time Shortening Effect of the Gd^{3+}-Containing Hybrid NPs. Gadolinium species with seven unpaired electrons are well-known candidates as positive contrast agents for magnetic resonance imaging (MRI) technique, as they can shorten the relaxation time of nearby water protons. By measuring the concentration-dependent longitudinal (T_1) and transverse relaxation time (T_2) at 37 °C and 7 T, the Gd^{3+}-containing silica hybrid NPs were investigated for their potential applications as contrast agents. From the plots of the longitudinal relaxation rate, $1/T_1$, against the Gd^{3+}-concentration (Figures 4A and B), the longitudinal relaxivity, r_1, of h-Gd_{3200} and h-Gd_{270} was determined as 12.7 and 12.2 $mmol^{-1}$ L s^{-1}, respectively (Table 3). Compared with

Table 3. Longitudinal (r_1) and Transverse Relaxivity (r_2) of the Gd^{3+}-Containing Silica Hybrid NPs Measured in D_2O at 37 °C and 7 T

hybrid	r_1 [$mmol^{-1}$ L s^{-1}]	r_2 [$mmol^{-1}$ L s^{-1}]	r_2/r_1
h-Gd_{3200}	12.7	52.8	4.1
h-Gd_{270}	12.2	44.6	3.6
h-Tb/Gd_{3200}	11.9	69.7	5.8

the commercial contrast agent gadopentetate dimeglumine (Gd-DTPA) possessing an r_1 value of 3.3 $mmol^{-1}$ L s^{-1} under the same conditions,[20] both h-Gd_{3200} and h-Gd_{270} exhibit much better T_1 contrast efficacy and can be used at a lower dose to achieve a comparable T_1 contrast enhancement. In the case of the multicomponent hybrid NP h-Tb/Gd_{3200} (Figure 4C), an r_1 value of 11.9 $mmol^{-1}$ L s^{-1} indicates that the incorporation of Tb^{3+} does not reduce the T_1 shortening effect and is harmless for potential MRI application. Combined with the Tb^{3+}-photoluminescence sensitized by Gd^{3+} (Figure 2F), h-Tb/Gd_{3200} can be used as dual imaging probe for MRI and fluorescence microscopy. It is to note that both T_1 and T_2 shortening effects can be observed in paramagnetic and superparamagnetic nanosystems, while the r_2/r_1 ratio is the

dx.doi.org/10.1021/cm402776d | Chem. Mater. 2013, 25, 4585−4594

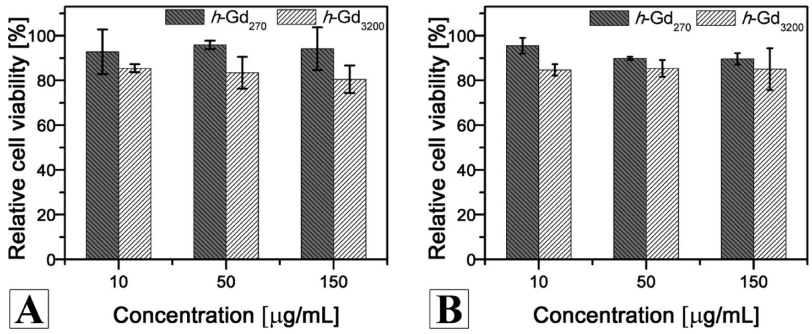

Figure 5. Relative viability of A549 cells incubated with the silica hybrid NPs h-Gd_{3200} and h-Gd_{270} of varying NP concentration with an incubation period of 24 h (A) and 72 h (B). The results are expressed as a percentage of the control cell culture.

most important factor to evaluate whether the material should be preferably applied as a positive contrast agent (T_1 shortening) or a negative one (T_2 shortening).[40] In general, the materials with low r_2/r_1 ratio are prevailing T_1 contrast agents. On the basis of the concentration-dependent T_1 and T_2 measurements, the r_2/r_1 ratio of h-Gd_{3200}, h-Gd_{270}, and h-Tb/Gd_{3200} was determined as 4.1, 3.6, and 5.8, respectively (Table 3). Compared with other reported gadolinium-containing nanomaterials (r_2/r_1 = 3.8−24.8),[20,40] our hybrid NPs have relatively low r_2/r_1, indicating that they are efficient T_1 contrast agents. Combined with their adequate solubility in water, the hybrid NPs are expected to exhibit a nice signal-to-noise ratio and a satisfying anatomical resolution in T_1-weighted MRI scans. MRI phantom images of water samples containing the hybrid NPs were recorded at 37 °C and 3 T to confirm their T_1 contrast efficacy. As shown in Figure 4D, the samples contrasted by h-Gd_{3200} or h-Gd_{270} were clearly detected, while a sample of pure water hardly demonstrated a T_1 signal. A comparison between the hybrid NPs and the commercial contrast agent Gd-DTPA was also performed. Even at a lower concentration of Gd^{3+} ions (0.20 mmol L^{-1}), both h-Gd_{3200} and h-Gd_{270} showed stronger T_1 contrast enhancement than the Gd-DTPA ([Gd^{3+}] = 0.36 mmol L^{-1}), suggesting the application perspective of the hybrid NPs as efficient MRI contrast agents. A comparison between the two hybrid NPs shows that the h-Gd_{3200} provides a slightly brighter signal at the same concentration (0.20 mmol L^{-1}), suggesting that a longer particle length results in a stronger T_1 contrast enhancement. In both cases of h-Gd_{3200} and h-Gd_{270}, the T_1 contrast effect increases expectedly with increasing concentration of the NPs.

Cytotoxicity of the Gd^{3+}-Containing Hybrid NPs. The cytotoxicity of the silica hybrid NPs h-Gd_{3200} and h-Gd_{270} was determined by cell culture using the human bronchoalveolar carcinoma derived cell line A549 as the tested cells. The MTT assay was used to assess the viability of the A549 cells after exposure to the hybrid NPs for 24 or 72 h at various concentrations of NP (10, 50, 150 μg mL^{-1}). As shown in Figure 5, the cell viability is not significantly altered (stays above 90%) after being incubated with h-Gd_{270} in the whole experimental period (72 h) regardless of the sample concentrations. The cell viability is slightly reduced when the cells were incubated with h-Gd_{3200} for 24 h. It is maintained above 80% of the NP-free control, although slightly decreased at higher concentrations. The cell viability stays relatively stable when the incubation time with h-Gd_{3200} extends to 72 h. All the results suggest that the silica hybrid NPs have a minimal toxicity to A549 cells. Another MTT assay of the human endothelial cells (CRL-1730) under incubation with the silica hybrid NPs h-Gd_{3200} and h-Gd_{270} was performed with an experimental period of 72 h. The results are shown in Figure S9 (SI). With a NP concentration of up to 150 μg mL^{-1}, the h-Gd_{270} shows only a minimal toxicity to endothelial cells. In the case of the h-Gd_{3200}, a very low toxicity to endothelial cells was observed at concentrations lower than 50 μg mL^{-1}. Furthermore, a MTT assay of a control sample of free Gd^{3+} ions was conducted by using the cell line A549, which indicates that the cell viability after exposure to free Gd^{3+} ions for 24 h at corresponding concentrations (10, 50, 150 μg mL^{-1}) is strongly reduced to ca. 65%. Therefore, the encapsulated hybrid NPs possess much lower cytotoxicity than the free Gd^{3+} ions. This minimal cytotoxicity of the silica hybrid NPs h-Gd_{3200} and h-Gd_{270} is attributed to the fact that all the toxic Gd^{3+} ions are tightly chelated in the PAA-core of the CPB template and are completely isolated by the cross-linked silica shell from the outside surrounding.

Another important characteristic of the silica hybrid NPs h-Gd_{3200} and h-Gd_{270} is the particle size and shape. As mentioned above, the h-Gd_{3200} and h-Gd_{270} has a mean particle length of 194 and 51 nm, respectively. NPs in this range of dimension not only extravasate from the leaky tumor vasculature to a higher degree than healthy tissue but also remain in the tumor issue by the enhanced permeability and retention (EPR) effect.[41−43] Under fluid flow conditions, due to the one-dimensional (1D) cylindrical shape of the hybrid NPs, they are taken up by cells less readily and more persistent than spheres, because the former are extended by the flow.[44] A combination of the adequate solubility in water, the significant T_1-shortening efficacy, the minimal cytotoxicity and the promising EPR effect suggests that the silica hybrid NPs h-Gd_{3200} and h-Gd_{270} can be applied as effective T_1 contrast agents for early stage cancer diagnose. Furthermore, it is noteworthy that the multi-component hybrid NP h-Tb/Gd_{3200} with combined visible photoluminescence and T_1 shortening effect is potential candidate for multimodal bioimaging.

■ CONCLUSIONS

Various well-defined rare-earth metal cations (Ln^{3+}) incorporated silica hybrid nanoparticles (NPs) with different particle sizes were successfully prepared via a template-directed approach based on core−shell cylindrical polymer brushes. The cross-linked silica shell deposited on the PDMAEMA segments ensures a high stability of the encapsulation of Ln^{3+} ions within the hybrid NPs, as well as a satisfying solubility in water and alcohols. Upon excitation with UV light, the silica hybrid NPs with Tb^{3+} or Eu^{3+} incorporation exhibit characteristic visible photoluminescence, which is sensitized by ligand or

dx.doi.org/10.1021/cm402776d | Chem. Mater. 2013, 25, 4585−4594

metal−metal energy transfer. SQUID measurements confirm the paramagnetic properties of the Gd^{3+} and Tb^{3+} containing silica hybrid NPs. Especially, the multicomponent hybrid NP incorporated with a mixture of Tb^{3+} and Gd^{3+} possesses both the visible photoluminescence and the paramagnetic property. The Gd^{3+}-containing silica hybrid nanoparticles show much higher longitudinal relaxivity, r_1, and stronger contrast enhancement in T_1-weighted MRI images than the commercial contrast agent Gd-DPTA. This remarkable T_1 shortening effect combined with a minimal cytotoxicity toward different human cells and a promising EPR effect suggests the potential application of the Gd^{3+}-containing silica hybrid NPs as effective MRI contrast agents for tumor diagnosis.

■ ASSOCIATED CONTENT

Supporting Information

Synthetic route, ^{1}H NMR spectra, AFM images, SEM images, EDX analysis, TGA results, etc. This material is available free of charge via the Internet at http://pubs.acs.org.

■ AUTHOR INFORMATION

Corresponding Authors

*E-mail: lingjun@zju.edu.cn.

*E-mail: axel.mueller@uni-mainz.de.

Present Address

[‖]Institute of Organic Chemistry, Johannes Gutenberg-Universität Mainz, D-55099 Mainz, Germany

Notes

The authors declare no competing financial interest.

■ ACKNOWLEDGMENTS

Z. Zheng appreciates a scholarship from the Elite Support Program of Bavaria. J. Ling sincerely thanks the Alexander von Humboldt Foundation for granting him a research fellowship and the National Science Foundation of China (No. 21374093). We thank Stephan Schlamp for SQUID measurements and Dr. Zhengwei Mao for cytotoxicity measurements.

■ REFERENCES

(1) McGill, I. Rare Earth Elements. In *Ullmann's Encyclopedia of Industrial Chemistry*; Wiley-VCH Verlag GmbH & Co. KGaA: Berlin/Heidelberg, 2000.

(2) Bünzli, J.-C. G.; André, N.; Elhabiri, M.; Muller, G.; Piguet, C. *J. Alloy. Compd.* **2000**, *303−304*, 66.

(3) Ma, Y.; Wang, Y. *Coordin. Chem. Rev.* **2010**, *254*, 972.

(4) Blasse, G.; Grabmaier, B. C. *Luminescent Materials*; Springer-Verlag: New York, 1994.

(5) Moeller, T. *J. Chem. Educ.* **1970**, *47*, 417.

(6) Zhang, H.; Xu, Y.; Yang, W.; Li, Q. *Chem. Mater.* **2007**, *19*, 5875.

(7) Carlos, L. D.; Ferreira, R. A. S.; Bermudez, V. d. Z.; Ribeiro, S. J. L. *Adv. Mater.* **2009**, *21*, 509.

(8) Zhou, J.; Sun, Y.; Du, X.; Xiong, L.; Hu, H.; Li, F. *Biomaterials* **2010**, *31*, 3287.

(9) Kenyon, A. J. *Prog. Quant. Electron.* **2002**, *26*, 225.

(10) Bunzli, J.-C. G.; Piguet, C. *Chem. Soc. Rev.* **2005**, *34*, 1048.

(11) Bouzigues, C.; Gacoin, T.; Alexandrou, A. *ACS Nano* **2011**, *5*, 8488.

(12) Bottrill, M.; Kwok, L.; Long, N. J. *Chem. Soc. Rev.* **2006**, *35*, 557.

(13) Carr, D. H.; Brown, J.; Bydder, G. M.; Steiner, R. E.; Weinmann, H.-J.; Speck, U.; Hall, A. S.; Young, I. R. *Am. J. Roentgenol.* **1984**, *143*, 215.

(14) Ye, M.; Qian, Y.; Shen, Y.; Hu, H.; Sui, M.; Tang, J. *J. Mater. Chem.* **2012**, *22*, 14369.

(15) Bridot, J.-L.; Faure, A.-C.; Laurent, S.; Rivière, C.; Billotey, C.; Hiba, B.; Janier, M.; Josserand, V.; Coll, J.-L.; Vander Elst, L.; Muller, R.; Roux, S.; Perriat, P.; Tillement, O. *J. Am. Chem. Soc.* **2007**, *129*, 5076.

(16) Hifumi, H.; Yamaoka, S.; Tanimoto, A.; Citterio, D.; Suzuki, K. *J. Am. Chem. Soc.* **2006**, *128*, 15090.

(17) Park, Y. I.; Kim, J. H.; Lee, K. T.; Jeon, K.-S.; Na, H. B.; Yu, J. H.; Kim, H. M.; Lee, N.; Choi, S. H.; Baik, S.-I.; Kim, H.; Park, S. P.; Park, B.-J.; Kim, Y. W.; Lee, S. H.; Yoon, S.-Y.; Song, I. C.; Moon, W. K.; Suh, Y. D.; Hyeon, T. *Adv. Mater.* **2009**, *21*, 4467.

(18) Hifumi, H.; Yamaoka, S.; Tanimoto, A.; Akatsu, T.; Shindo, Y.; Honda, A.; Citterio, D.; Oka, K.; Kuribayashi, S.; Suzuki, K. *J. Mater. Chem.* **2009**, *19*, 6393.

(19) Liu, Q.; Sun, Y.; Li, C.; Zhou, J.; Li, C.; Yang, T.; Zhang, X.; Yi, T.; Wu, D.; Li, F. *ACS Nano* **2011**, *5*, 3146.

(20) Zhou, Z.; Wang, L.; Chi, X.; Bao, J.; Yang, L.; Zhao, W.; Chen, Z.; Wang, X.; Chen, X.; Gao, J. *ACS Nano* **2013**, *7*, 3287.

(21) Zhang, M.; Estournès, C.; Bietsch, W.; Müller, A. H. E. *Adv. Funct. Mater.* **2004**, *14*, 871.

(22) Xu, Y.; Yuan, J.; Fang, B.; Drechsler, M.; Müllner, M.; Bolisetty, S.; Ballauff, M.; Müller, A. H. E. *Adv. Funct. Mater.* **2010**, *20*, 4182.

(23) Yuan, J.; Xu, Y.; Walther, A.; Bolisetty, S.; Schumacher, M.; Schmalz, H.; Ballauff, M.; Müller, A. H. E. *Nat. Mater.* **2008**, *7*, 718.

(24) Müllner, M.; Yuan, J.; Weiss, S.; Walther, A.; Förtsch, M.; Drechsler, M.; Müller, A. H. E. *J. Am. Chem. Soc.* **2010**, *132*, 16587.

(25) Müllner, M.; Lunkenbein, T.; Breu, J.; Caruso, F.; Müller, A. H. E. *Chem. Mater.* **2012**, *24*, 1802.

(26) Zhang, M.; Drechsler, M.; Müller, A. H. E. *Chem. Mater.* **2004**, *16*, 537.

(27) Yuan, J.; Schacher, F.; Drechsler, M.; Hanisch, A.; Lu, Y.; Ballauff, M.; Müller, A. H. E. *Chem. Mater.* **2010**, *22*, 2626.

(28) Yuan, J.; Lu, Y.; Schacher, F.; Lunkenbein, T.; Weiss, S.; Schmalz, H.; Müller, A. H. E. *Chem. Mater.* **2009**, *21*, 4146.

(29) Müllner, M.; Lunkenbein, T.; Schieder, M.; Gröschel, A. H.; Miyajima, N.; Förtsch, M.; Breu, J.; Caruso, F.; Müller, A. H. E. *Macromolecules* **2012**, *45*, 6981.

(30) Zhang, M.; Breiner, T.; Mori, H.; Müller, A. H. E. *Polymer* **2003**, *44*, 1449.

(31) Venkatesh, R.; Yajjou, L.; Koning, C. E.; Klumperman, B. *Macromol. Chem. Phys.* **2004**, *205*, 2161.

(32) Plamper, F. A.; Schmalz, A.; Penott-Chang, E.; Drechsler, M.; Jusufi, A.; Ballauff, M.; Müller, A. H. E. *Macromolecules* **2007**, *40*, 5689.

(33) Retsch, M.; Walther, A.; Loos, K.; Müller, A. H. E. *Langmuir* **2008**, *24*, 9421.

(34) Yuan, J.-J.; Mykhaylyk, O. O.; Ryan, A. J.; Armes, S. P. *J. Am. Chem. Soc.* **2007**, *129*, 1717.

(35) Li, Y.; Du, J.; Armes, S. P. *Macromol. Rapid Commun.* **2009**, *30*, 464.

(36) Huang, C.-C.; Liu, T.-Y.; Su, C.-H.; Lo, Y.-W.; Chen, J.-H.; Yeh, C.-S. *Chem. Mater.* **2008**, *20*, 3840.

(37) Liu, D.; Yu, H.; Wang, Z.; Nie, Q. *Polym. Int.* **2010**, *59*, 937.

(38) Li, H. R.; Lin, J.; Zhang, H. J.; Fu, L. S.; Meng, Q. G.; Wang, S. B. *Chem. Mater.* **2002**, *14*, 3651.

(39) Li, Y.-C.; Chang, Y.-H.; Chang, Y.-S.; Lin, Y.-J.; Laing, C.-H. *J. Phys. Chem. C* **2007**, *111*, 10682.

(40) Kim, B. H.; Lee, N.; Kim, H.; An, K.; Park, Y. I.; Choi, Y.; Shin, K.; Lee, Y.; Kwon, S. G.; Na, H. B.; Park, J.-G.; Ahn, T.-Y.; Kim, Y.-W.; Moon, W. K.; Choi, S. H.; Hyeon, T. *J. Am. Chem. Soc.* **2011**, *133*, 12624.

(41) Alexis, F.; Pridgen, E.; Molnar, L. K.; Farokhzad, O. C. *Mol. Pharmaceutics* **2008**, *5*, 505.

(42) Jokerst, J. V.; Lobovkina, T.; Zare, R. N.; Gambhir, S. S. *Nanomedicine* **2011**, *6*, 715.

(43) Maeda, H.; Wu, J.; Sawa, T.; Matsumura, Y.; Hori, K. *J. Controlled Release* **2000**, *65*, 271.

(44) Geng, Y.; Dalhaimer, P.; Cai, S.; Tsai, R.; Tewari, M.; Minko, T.; Discher, D. E. *Nat. Nano.* **2007**, *2*, 249.